# Asymmetric Flasklike Hollow Carbonaceous Nanoparticles Fabricated by the Synergistic Interaction between Soft Template and Biomass

Chunhong Chen, Haiyan Wang, Chuanlong Han, Jiang Deng, Jing Wang, Mingming Li, Minghui Tang, Haiyan Jin, and Yong Wang*

Advanced Materials and Catalysis Group, ZJU-NHU United R&D Center, Department of Chemistry, Zhejiang University, Hangzhou 310028, P. R. China

S *Supporting Information*

ABSTRACT: The soft template method is broadly applied to the fabrication of hollow-structured nanomaterials. However, due to the instability and the typical spherical shape of these soft templates, the resultant particles have a spherical morphology with a wide size distribution. Herein, we developed a sustainable route to fabricate asymmetric flasklike hollow carbonaceous structures with a highly uniform morphology and a narrow size distribution using the soft template method. A dynamic growth mechanism induced by the synergetic interactions between template and biomass is proposed. The precursors (ribose) provide an acidic environment for sodium oleate during the hydrothermal process in which oleic acid nanoemulsions are initially formed and serve as both template and benign solvent for the amphiphilic derivatives of the precursor. Simultaneously, the cosurfactant P123 facilitates the uniform dispersion of the nanoemulsion and is believed to cause the carbonaceous shells to rupture, providing openings through which the intermediates can enter. These subtle interactions facilitate the formation of the flasklike, asymmetric, hollow, carbonaceous nanoparticles. Furthermore, this unique structure contributes to the high surface area (2335 m² g⁻¹) of the flasklike carbon particles, which enhances the performance of supercapacitors. These findings may open up an exciting field for exploring anisotropic carbonaceous nanomaterials and for understanding the related mechanisms to provide guidance for the design of increasingly complex carbonaceous materials.

Nanofabrication

VS

- nanoscale
- flasklike
- carbon
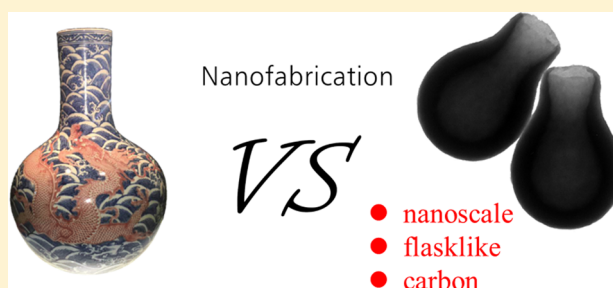
INTRODUCTION

The past few decades have witnessed an unprecedented revolution in nanomaterial synthesis, which has given rise to remarkable building blocks with different structures, compositions, and shapes. The design and fabrication of hollow nanoparticles, including silica, metal oxides, polymers, and carbonaceous materials, have received considerable attention in both fundamental research and practical applications.[1−5] Benefiting from the merits of low density, high surface area, and large cavities, these hollow particles present promising application prospects in catalysis, drug storage and release, and energy storage.[6−9] Among the various morphologies of the hollow nanoparticles investigated, asymmetric nanoparticles, such as cage-structured, bowl-shaped, and other patterned nonspherical particles,[10−15] have become a focus because of the subtle combination of the hollow structure with the distinctive asymmetric architecture. For example, asymmetric particles can be benign carriers for temperature-controlled drug delivery or essential building blocks for the fabrication of energy storage systems with improved energy density.[16,17] Despite the considerable endeavors devoted to the fabrication of these materials, only a few methods, such as freeze-drying and freeze-

etching, anisotropic encapsulation, and template-engaged chemical etching,[15,17,18] have been reported for the preparation of asymmetric hollow nanoparticles. In addition, most of the asymmetric hollow nanoparticles reported are limited to silica, polymer latex (e.g., polystyrene), or metal oxides, whose synthetic routes are lengthy and typically involve toxic organic polymers or caustic reagents. Because of the advantages of large voids, good biocompatibility, chemical inertness, and high conductivity, hollow-structured carbonaceous materials have been extensively investigated.[19−22] However, they are mostly spherical in shape. Thus, preparing asymmetric hollow carbonaceous structures remains a great challenge.

Several methods have been developed for the fabrication of hollow carbonaceous spheres. Traditionally, hard template methods employing silica, metals, or metal compounds as the hard templates are typically used for the fabrication of hollow carbonaceous spheres.[7,23−26] Unfortunately, the process involves multiple steps, as it inevitably requires the aggressive chemical etching of hard templates. Compared with the hard

template method, the soft template method is simple and feasible. The soft template route refers to the direct generation of hollow structures via self-assembly between the precursor molecules and core templates. Organic surfactants, block copolymers, or nanoemulsion droplets usually act as the cores and can be gently consumed or removed in the subsequent calcination procedure.[27−29] However, these precursors in the soft template method are usually limited to those that easily polymerize at low temperatures, such as phenolic resin. When referring to sustainable precursors, such as biomass and its derivatives,[30] only a few studies based on the soft template method have been reported.[31,32] The resultant hollow spheres are inhomogeneous in shape and have a wide size distribution, primarily because of the thermodynamic instability of these soft cores and the weak self-assembly ability between templates and precursors using the high-temperature hydrothermal approach (usually 160−200 °C).[19,33] The biomass-derived hollow carbonaceous spheres based on the soft template method have undergone limited development, and even less development has occurred for the asymmetric ones. Thus, it remains an intriguing challenge to realize the precise fabrication of asymmetric hollow morphologies from biomass-derived precursors via the soft template method.

In this contribution, the difficult task of fabricating asymmetric hollow carbon nanoparticles was accomplished based on inexpensive and naturally available sugars through a very simple, one-pot, soft template, hydrothermal synthesis. These obtained products have flasklike hollow shapes with a single opening in the shells; for simplicity, they are named hollow, open, carbonaceous nanoflasks (HOCFs). The unexpected versatile abilities of this novel, open morphology are quickly recognized and contribute significantly to the application of the products. Flasklike carbon particles with a large surface area of 2335 m^2 g$^{−1}$ are obtained after subsequent carbonization using a novel "leavening" strategy.[34,35] The unique porous structure is shown to enhance the performance of supercapacitors.

■ RESULTS AND DISCUSSION

Poly(ethylene glycol)-*block*-poly(propylene glycol)-*block*-poly-(ethylene glycol) (EO$_{20}$-PO$_{70}$-EO$_{20}$, P123) and sodium oleate (SO) were chosen as double surfactants, and ribose was selected as the carbon source. The hydrophobic interactions between the PPO (poly(propylene oxide)) blocks of P123 and the alkyl chains of SO can cause the formation of mixed micelles in aqueous media.[36,37] The dynamic light scattering (DLS) results confirmed the strong interaction between P123 and SO since the micelle size decreased from 12 to 1 nm, as shown in Figure S1. The observation that the critical micelle concentration of mixed micelles was less than that of pure SO also confirmed the copolymer−surfactant interaction (Figure S2).[37] Ribose, a type of biomass derivative, is well-known as a carbon precursor under hydrothermal conditions. The detailed fabrication steps are as follows: the SO and P123 solution was homogeneously mixed with ribose, then the mixture was transferred to an autoclave and hydrothermally aged for 12 h, followed by centrifugation with deionized water and drying in the oven. The final product was denoted as HOCFs-12.

A scanning electron microscopy (SEM) image of the obtained HOCFs-12 showed the uniform and round-bottom flasklike morphology (Figure 1a). The HOCFs-12 have a uniform body size of ∼500 nm, with an unambiguously open neck (Figure S3a). The transmission electron microscopy
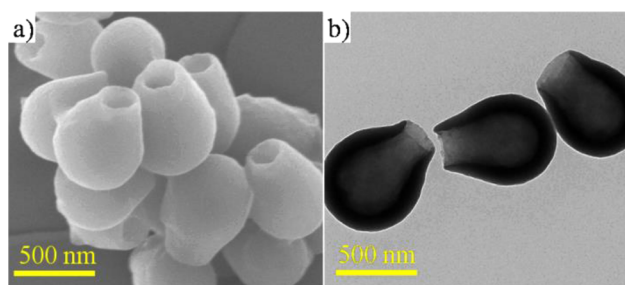

Figure 1. Morphologies of HOCFs: (a) SEM and (b) TEM images of the HOCFs-12.

(TEM) image (Figure 1b) clearly showed the hollow flasklike shapes with a single opening at the end of the necks; interestingly, the diameters of the hollow cavities can reach ∼400 nm (Figure S3b). Both the SEM and TEM images revealed that asymmetric, hollow, unique carbonaceous nanomaterials were successfully prepared.

The shape evolution was first studied by varying the hydrothermal reaction time, and the corresponding samples were denoted as HOCFs-*x* (*x* refers to the hydrothermal reaction time of 8, 12, 21, and 24 h). The morphologies and sizes of these nanoparticles were examined by TEM and SEM (Figure 2). As shown in Figure 2, almost all the products were uniformly dispersed, whereas obvious morphology differences were observed for different hydrothermal times. For HOCFs-8 (Figure 2a and 2e), hollow spheres with a single hole in the surface of each particle were observed. When the hydrothermal treatment time was extended, significant distinctions appeared: open spheres evolved into flasklike structures (Figure 2b−d and 2f−h) and the length of the neck increased with the reaction time. Meanwhile, another clear trend was that the diameter of the inner cavity gradually decreased. As listed in Figure 2i−l, the average diameters of the inner cavities decreased from approximately 401 to 229 nm with a prolonged hydrothermal reaction time. Therefore, the following conclusions can be obtained from the evolution: openings were formed at an early stage, the growth of the necks indicated the newly emerging templates over time, and the decreased diameters of the hollow voids revealed that polymerization in the cores was occurring successively.

As mentioned above, the diameters of the inner cavities can reach approximately 400 nm. According to the molecular structure, the theoretical size of the two surfactants would be no more than dozens of nanometers.[38] To reveal the specific roles of the two surfactants, a series of supplementary experiments was designed. Different ratios between SO and P123 were added while keeping the other reaction conditions the same as those used to prepare HOCFs-12. Diverse morphologies were presented (Figure 3a−e). The obtained products synthesized using the ratio of 16:0 (indicating no P123, Figure 3a) showed intact nanospheres with a wide size distribution from several tens of nanometers to hundreds of nanometers. Meanwhile, the diameters of the hollow cores also reached hundreds of nanometers. As is known, SO, a strong base−weak acid salt, can be hydrolyzed easily and can produce oleic acid in dilute aqueous solutions.[37] Therefore, an acid (oleic acid) and an anion (oleate) might coexist. In addition, it is well-known that not only polymerization reactions but also decomposition reactions occur when saccharides are treated at sub- or supercritical water temperatures ranging from 150 to 350 °C. The decomposition of the monosaccharide leads to the
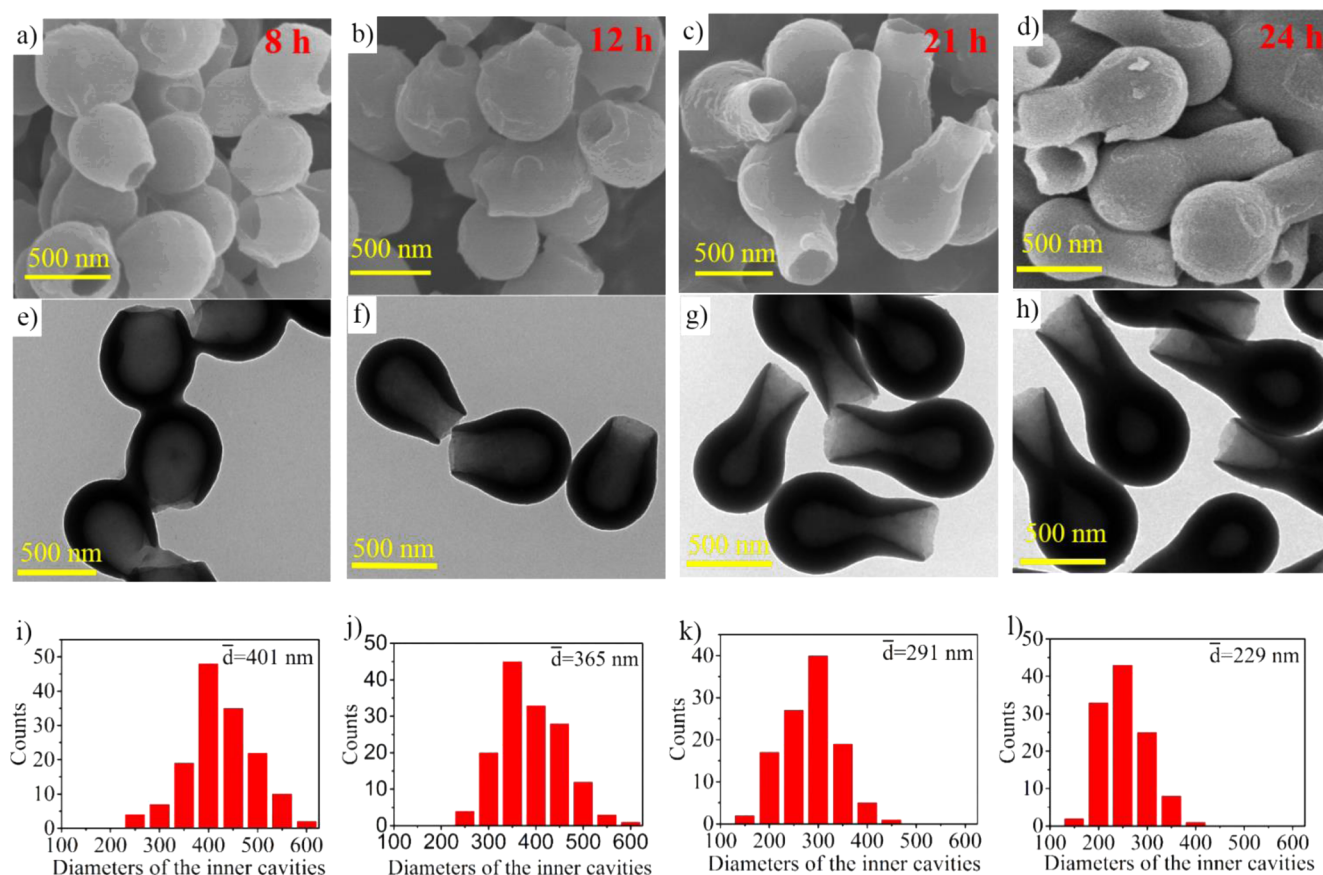
Figure 2. (a−d) SEM and (e−h) TEM images of the HOCFs prepared with different hydrothermal times. (i−l) Corresponding distribution histograms of the diameters of the inner cavities at different times (inset d is the average diameter). The hydrothermal times were (a, e, i) 8 h, (b, f, j) 12 h, (c, g, k) 21 h, and (d, h, l) 24 h.
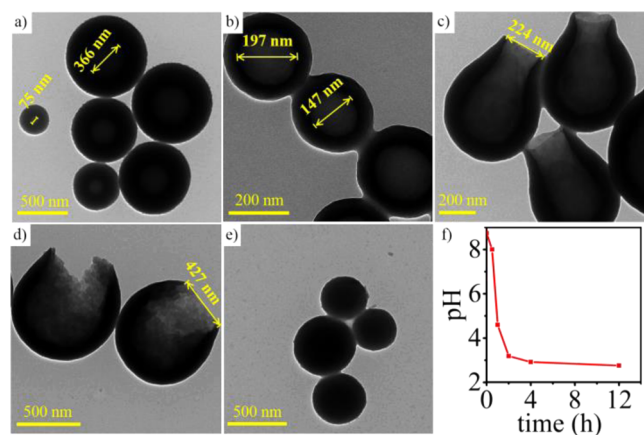
Figure 3. TEM images of the corresponding morphologies synthesized with different molar ratios of SO and P123: (a) 16:0 (without P123), (b) 16:0.5, (c) 16:1, (d) 16:2, (e) 0:1 (without SO). Note: the diameters of the hollow polymer spheres are labeled in (a, b), and the diameters of the openings are labeled in (c, d); (f) pH dependence of the hydrothermal reaction time.

formation of organic acids (e.g., acetic acid, lactic acid, and formic acid), which decrease the pH of the reaction solution.[39,40] In this case, oleate would be converted to oleic acid with a decrease in pH. The solubility of oleic acid is only 2.51×10^{-8} mol L^{-1} in water.[41] Thus, oleic acid can precipitate and aggregate easily, forming oleic acid nanoemulsions with an increase in the temperature, which minimizes the surface

energy. This deduction can well explain the ultra large cores (oleic acid nanoemulsions) in the pure SO system (Figure 3a, 366 nm). In addition, polymerization of ribose could occur at the interface of the oleic acid emulsion and water, which can impede the further growth of the oleic acid emulsion, therefore inhibiting the phase separation of oleic acid. When a small amount of P123 was added to SO (16:0.5), relatively uniform hollow spheres formed (Figure 3b). The different morphologies (Figure 3a and Figure 3b) further indicated that P123 strongly interacted with SO. P123 served as a surfactant for the stabilization and dispersion of the oleic acid emulsions, leading to a narrower size distribution of the nanoemulsions. When the amount of P123 was doubled (16:1, HOCFs-12), flasklike, hollow, carbonaceous nanoparticles with open necks were obtained (Figure 3c). Upon further increasing the amount of P123 (16:2), the diameter of the openings was obviously enlarged compared with that of HOCFs-12 (Figure 3d, 427 versus 224 nm). It has been reported that the PPO blocks of the Pluronic triblock copolymers present hydrophobicity above approximately 15 °C. For PEO blocks (poly(ethylene glycol)), the hydration level decreases as the temperature increases, especially at temperatures over 100 °C because of the breakage of hydrogen bonds between PEO and water.[42,43] Hence, in addition to the anchoring of the PPO blocks of P123 in the nanoemulsion from the beginning (with hydrophobic interactions as the driving force), the PEO blocks tend to penetrate into the oleic acid nanoemulsions at elevated temperatures, further reducing the interface energy. Noticeably, the penetration of the PEO blocks into the nanoemulsion can

cause a volume expansion of the intrananoemulsions, which can then induce some tensile stress.[12,44] Meanwhile, polymerization of ribose on the template would occur, forming carbonaceous shells. Therefore, the pressure (exceeding one critical pressure) from the volume expansion of the inner nanoemulsion would eventually lead to cracking of the oligomer shells. The increase in the P123 content (the amounts of ribose and sodium oleate were constant) caused an increase in pressure (Figure S5), therefore offering control over the diameter of the openings. With only the addition of P123, solid nanoparticles were produced (Figure 3e). Thus, we concluded that ribose can strongly associate with the template and polymerize with hollow patterns only in the presence of SO under hydrothermal conditions. This result also revealed that oleic acid nanoemulsions can provide an oil-phase environment for P123. In turn, P123 present in oleic acid promoted the dispersion of the nanoemulsions. Then, the two surfactants worked together and performed their respective functions in the polymerization of ribose at a high temperature.

To verify the transformation from SO to oleic acid nanoemulsions, the pH values of the HOCFs solutions were tested before centrifugation (Figure 3f), and the turbidity changes were recorded using photographs at different stages (Figure S6). Generally, the pH values decreased with the hydrothermal time. The pH value of the sample before hydrothermal treatment was approximately 8.74, and the solution of the sample was almost transparent (Figure S6a). After only 0.5 h of reaction time, the pH decreased to approximately 8.00, and the solution turned milky (Figure S6b). The mean DLS value for this milky solution was approximately 134.5 nm, which should be attributed to the formation of oleic acid nanoemulsions from SO (Table S1, a detailed discussion is presented in the Supporting Information). As the hydrothermal treatment was extended to 1 h, the pH value sharply dropped to 4.65, and the solution resembled a clay bank, indicating the polymerization of ribose (Figure S6c). It is worth mentioning that oleic acid would be precipitated from water via aggregation under acidic and high-temperature conditions in the absence of ribose (Figure S8). Thus, the polymerization of ribose at the water−nanoemulsion interface successfully prevented the constant aggregation between the internanoemulsions. As the treatment time was prolonged to 12 h, the pH decreased slowly to 2.76. This trend has been confirmed in previous studies, showing that the pH value decreases sharply in the early stage and then levels off.[40] On the basis of the above analysis, we conclude that oleic acid nanoemulsions formed during the early stage under acidic conditions, and they acted as templates for the polymerization of ribose. Notably, the acid was formed by the decomposition of ribose, and the further aggregation of nanoemulsions was inhibited by the polymerization of ribose. These results revealed that the synergistic interaction in addition to the self-assembly between SO and ribose prompted the formation of the hollow-structured materials.

As revealed by the shape evolution with the hydrothermal reaction time, the new template surfaces gradually emerged, and the diameters of the inner cores decreased. Thus, it is reasonable to suppose that a substance entered the core gradually and polymerized there, which in turn led to the outflow of the nanoemulsion and the continuous decrease in the cavity diameter. In practice, it is widely accepted that ribose derivatives, such as furfural and oligomers, show limited solubility during hydrothermal processes.[39] Hence, we ascribed

this unique evolution to the two-phase (oil/water) distribution constants of these derivatives (K, Table S2). The K values (approximately 1−2 for furfural) of the derivatives reveal that they can exist in aqueous solutions (in the water phase) and can dissolve in intraemulsions (in the oil phase). These derivatives continuously filled in the cavities (they dissolve in the oil phase) from the aqueous solution, resulting in the gradual outflow of the nanoemulsions from the cavities; these derivatives then polymerized along the inner interface, leading to a decrease in the inner diameters. Meanwhile, the nanoemulsions that flowed out can form a fresh water−oil interface (the new soft templates). Once the new interface is formed, partial intermediates can self-assemble and polymerize along the newly formed surface of the two phases. This nucleation should occur along the rim of the established polymer wall, leading to the growth of necks. The above filling and outflow process can occur repeatedly, eventually leading to the growth of the necks. These deductions are in accordance with our experimental phenomena in which the necks of nanoflasks were extended and the hollow voids were narrowed. Certainly, the presence of these openings at the end of the necks allowed the structures to be continuously filled by the derivatives. Without these openings (prepared with only SO), only hollow spheres would be obtained. Thus, from the evidence above, we conclude that both the openings created by P123 and the solubility of the derivatives in oil (the oleic acid nanoemulsions) contributed to the formation and growth of necks.

On the basis of the above study, we proposed that the formation of the HOCFs includes three main stages, as shown in Figure 4: the formation of the nanoemulsions, the openings,
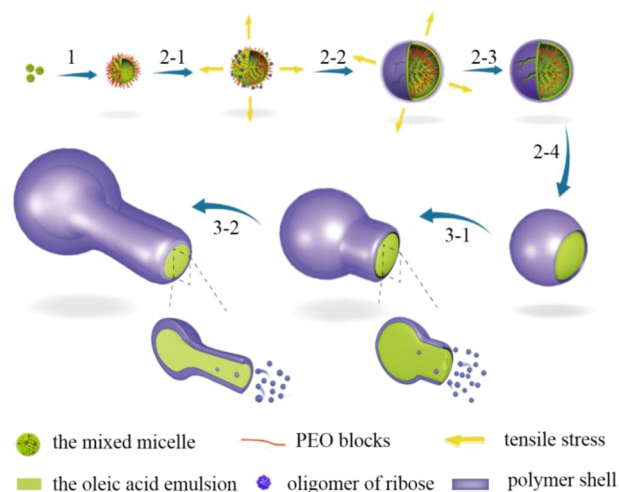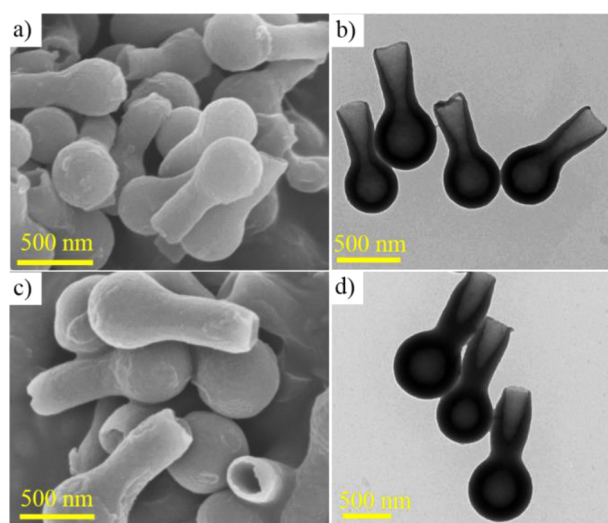

Figure 4. Schematic growth mechanism of the HOCFs. (1) Formation of nanoemulsions: Oleic acid formed and aggregated. (2) Formation of openings: (2-1, 2-2) PEO blocks caused the nanoemulsions to swell, (2-3, 2-4) and the shells were cracked by the tensile stress. (3) Formation of necks: The derivatives filled in, and the nanoemulsion flowed out gradually.

and the necks. During the first stage, mixed micelles are initially formed, and then they aggregate as nanoemulsions (oleic acid as the core and P123 as the surfactant) as the pH decreases and the temperature increases (step 1). As time progresses, the polymerization of ribose occurs, and further aggregation between nanoemulsions is inhibited (2-1). Meanwhile, the PEO blocks become more hydrophobic and start to cause

swelling of the nanoemulsion. The volume expansion of the nanoemulsions imposes a tensile stress (2-1, 2-2), eventually causing the polymer shell to crack (2-3, 2-4). At the final stage (step 3), some of the derivatives gradually dissolve into the oleic acid phase through the as-formed openings due to their solubility. Therefore, polymerization of derivatives would occur along the inner surface, thus reducing the inner diameter. The continuous filling process causes the outflow of the nano-emulsion, forming a fresh template surface. Thus, nucleation and polymerization would also occur along the newly formed template surface, causing a lengthening of the necks of the nanoflasks. In summary, we presented a reasonable mechanism in which synergetic interactions between template and biomass induced a dynamic process. These subtle interactions facilitate the formation of the HOCFs.
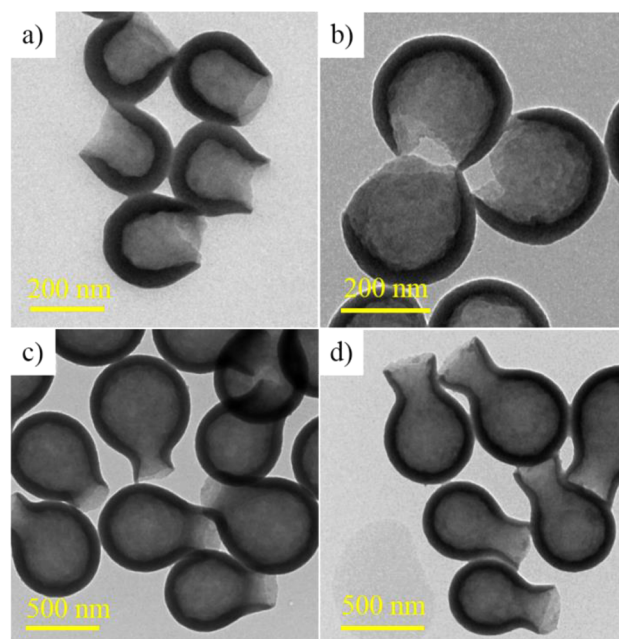
The synthesis method can be applied to other biomasses. Following the HOCFs-24 fabrication steps, we attempted to use arabinose (Figure 5a and 5b) and xylose (Figure 5c and

Figure 6. TEM images of the asymmetric nanoparticles derived from different mixed surfactants: (a) SDS and P123, (b) SDS and F127, (c) sodium stearate and P123, and (d) sodium laurate and P123.

Figure 5. SEM and TEM images of the structures of arabinose (a, b) and xylose (c, d).

5d). These sugars also resulted in shapes similar to those of HOCFs. Moreover, we extended this procedure to other double soft templates (such as sodium dodecyl sulfate (SDS)/P123, SDS/F127, sodium stearate/P123, and sodium laurate/P123). As shown in Figure 6, all the nanoparticles exhibited similar structures. Hence, the proposed synergetic interaction between templates and biomass can be considered a general mechanism.

The unusual integration of hollow, open, and carbonaceous characteristics provided an unprecedented opportunity to enhance the performance of HOCFs in supercapacitors, as they were strongly associated with the availability of pores during charge storage and ion transport. As shown in Figure S9, porous, hollow, open, carbon nanoflasks (PHOCFs) were obtained by the subsequent carbonization of HOCFs at 900 °C with the aid of foaming agents. The specific surface area and total pore volume were calculated as 2335 m^2 g^{-1} and 1.34 cm^3 g^{-1}, respectively (Figure S11), suggesting their great potential for use in supercapacitors. As a demonstration, the electro-chemical performance of PHOCFs was tested using a symmetric two-electrode system in a 6 M KOH solution. The cyclic voltammetry (CV) curves exhibited nearly

rectangular shapes over a wide range from 10 to 1000 mV s^{-1}, indicating the nearly ideal capacitive behavior of PHOCFs (Figure 7a). Figure 7b shows the typical triangular shapes of
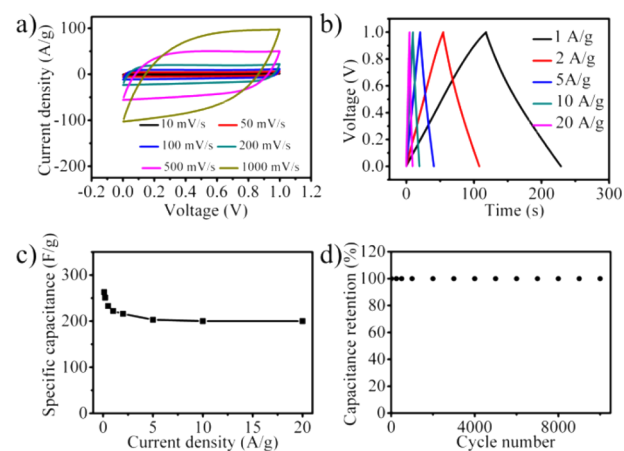
Figure 7. Supercapacitive performances of PHOCFs: (a) CV curves at various sweep rates and (b) galvanostatic charge–discharge curves at different current densities for PHOCFs. (c) Specific capacitances of PHOCFs calculated based on galvanostatic charge–discharge tests. (d) Cyclic stability of PHOCFs at 20 A g^{-1} over 10 000 cycles.

galvanostatic charge/discharge (GCD) curves, further manifest-ing an efficient electric double layer and fast ion transport within the open and porous electrodes. The specific capacitance of PHOCFs was calculated as 263 F g^{-1} at 0.1 A g^{-1} and maintained 222 F g^{-1} at 1 A g^{-1} (Figure S12), which are among the best values reported for porous carbon materials (Table S4). In addition, a high rate capability with 76% capacitance retention was obtained with a 200-fold increase in current density (Figure 7c). This result was due to the fast ion transport of PHOCFs by integrating the advantages of open and porous shells, as manifested by the small charge transfer

resistance (0.19 Ω) in the electrochemical impedance spectra (Figure S13). An energy density of 9.13 Wh kg^{-1} was obtained, which is higher than that of commercial supercapacitors (5 Wh kg^{-1}). Additionally, PHOCFs showed no decrease in capacitance after 10000 cycles at 20 A g^{-1} (Figure 7d). These results reveal the great potential of PHOCFs in electrochemical cells for electric power applications.

CONCLUSION

In summary, asymmetric, hollow, open, carbonaceous nanoflasks with a narrow size distribution were successfully fabricated. To the best of our knowledge, this is the first report on the synthesis of these unique carbonaceous nanostructures, which could represent a new type of carbonaceous nanomaterial. On the basis of the controlled experimental analysis, the formation mechanism was well studied and proposed in which synergetic interactions between template and biomass induced a dynamic process. This study presents a new avenue for the design and construction of anisotropic yet well-defined carbonaceous nanostructures. In addition, the results enable access to achieve inspirational methodology for the increasingly complex carbonaceous materials. The HOCFs can be carbonized to both porous and open carbon structures, and they show enhanced electrochemical performance in supercapacitors. We believe the unique combination of hollow carbon particles derived from biomass and the well-defined flasklike morphology may present new possibilities to create a class of original nanocarriers suitable for a variety of practical applications in medicine, energy, and catalysis.

EXPERIMENTAL SECTION

Materials. P123 was purchased from Sigma-Aldrich. SO, 98%, D-ribose (98%), furfural (99%), and oleic acid (98%) were supplied by Aladdin. $(NH_4)_2C_2O_4 \cdot H_2O$ (AR) and $KHCO_3$ (AR) were purchased from Sinopharm Chemical Reagent Co., Ltd. All chemicals were used as received without any further purification.

Synthesis of Hollow, Open, Carbonaceous Nanoflasks. In a typical procedure, 0.12 mmol SO and 0.0075 mmol P123 were dissolved in 20 mL of deionized water and stirred slowly to form a clear solution. Then 40 mL of an aqueous solution containing 3 g of ribose was added. The mixture formed an almost transparent solution after stirring for 30 min at room temperature. The resultant solution was transferred into an autoclave (approximately 85 mL) and hydrothermally treated at 160 °C for 12 h. After the autoclave cooled to room temperature, the solid products were collected by centrifugation (9500 rpm, 15 min), washed three times with deionized water, and dried at 70 °C overnight.

Synthesis of PHOCFs. Interestingly, our experiment can be magnified by 10 times with the products maintaining their original morphology. For further optimization, the reaction time was prolonged to 16 h, denoted as HOCFs-16. Additional carbonation modifications were performed according to our reported work.[35] Typically, a mixture of HOCFs-16, $(NH_4)_2C_2O_4 \cdot H_2O$, and $KHCO_3$ (mass ratio of 1:4:4) was mixed thoroughly by grinding for 30 min. Then the mixture was calcined to 600 °C at a heating rate of 10 °C min^{-1} and was held at that temperature for 1 h under N_2 atmosphere. The sample was then further heated to 900 °C at a rate of 5 °C and kept for 1 h. After the sample was cooled, the black powder was dissolved in an acid aqueous solution and stirred for 12 h. The porous HOCFs (PHOCFs) were obtained after the powder solution was washed with deionized water several times and dried in an oven overnight.

Characterization. TEM was carried out with a Hitachi HT-7700 microscope. The samples were prepared by dipping the carbon-coated copper grids into ethanol solutions of the products and drying at room temperature. SEM images were obtained using a Hitachi S-4800 and Hitachi SU-70. DLS measurements were recorded on a Malvern Zetasizer Nano-ZS using laser radiation with a wavelength of 633 nm and a power of 4 mW. The scattered light was measured at a backscattering angle of 173°. An HPLC instrument equipped with a refractive index (RI) detector and a sapphire C18 column was used to measure the oil (oleic acid)/water distribution constant (K) of furfural. The N_2 adsorption−desorption isothermal analysis was performed using a Micromeritics ASAP 2020 HD88, and the surface area was calculated using the BET equation. Surface tension measurements were obtained on a Dataphysics OCA20.

Electrochemical Measurements for Supercapacitors. The electrochemical performances of PHOCFs-16 were investigated and carried out in 6 M KOH electrolyte using a symmetric two-electrode test system. A mixture of the carbon samples and polytetrafluoroethylene in a weight ratio of 9:1 was dropped onto nickel foam. The carbon-casted nickel foam was pressed under 10 MPa for 5 min after air drying, and the density of carbon materials per electrode was approximately 2.5 mg cm^{-2}. Two electrodes were soaked in 6 M KOH electrolyte. All the electrochemical measurements were performed on a Gamry Reference 600 electrochemical workstation at room temperature. Electrochemical impedance spectroscopy was performed at open circuit potential over the frequency range from 0.01 to 100 Hz with an amplitude of 5 mV.

ASSOCIATED CONTENT

S Supporting Information

The Supporting Information is available free of charge on the ACS Publications website at DOI: 10.1021/jacs.6b10841.

> DLS of the surfactants, surface tension measurements, TEM images of the HOCFs-x, TEM images of the morphologies derived from different SO to P123 ratios, photos and pH values of the reaction solution, distribution constant of furfural at different temperatures, electrochemical performance of PHOCFs and PHCS (PDF)

AUTHOR INFORMATION

Corresponding Author

*chemwy@zju.edu.cn.

ORCID 🄔

Minghui Tang: 0000-0002-3384-8628

Yong Wang: 0000-0001-8043-5757

Notes

The authors declare no competing financial interest.

ACKNOWLEDGMENTS

REFERENCES

(1) Chen, M.; Wu, L.; Zhou, S.; You, B. *Adv. Mater.* **2006**, *18*, 801.

(2) Titirici, M.-M.; Antonietti, M.; Thomas, A. *Chem. Mater.* **2006**, *18*, 3808.

(3) Zhou, W.; Gao, H.; Goodenough, J. B. *Adv. Energy Mater.* **2016**, *6*, 150182.

(4) Xiao, Q.; Gu, M.; Yang, H.; Li, B.; Zhang, C.; Liu, Y.; Liu, F.; Dai, F.; Yang, L.; Liu, Z.; Xiao, X.; Liu, G.; Zhao, P.; Zhang, S.; Wang, C.; Lu, Y.; Cai, M. *Nat. Commun.* **2015**, *6*, 8844.

(5) Hofer, C. J.; Grass, R. N.; Zeltner, M.; Mora, C. A.; Krumeich, F.; Stark, W. J. *Angew. Chem., Int. Ed.* **2016**, *55*, 8761.

(6) Hung, L.-I.; Tsung, C.-K.; Huang, W.; Yang, P. *Adv. Mater.* **2010**, *22*, 1910.

(7) Liu, R.; Mahurin, S. M.; Li, C.; Unocic, R. R.; Idrobo, J. C.; Gao, H.; Pennycook, S. J.; Dai, S. *Angew. Chem., Int. Ed.* **2011**, *50*, 6799.

(8) Shen, L.; Yu, L.; Yu, X.-Y.; Zhang, X.; Lou, X. W. *Angew. Chem., Int. Ed.* **2015**, *54*, 1868.

(9) Teng, Z.; Wang, S.; Su, X.; Chen, G.; Liu, Y.; Luo, Z.; Luo, W.; Tang, Y.; Ju, H.; Zhao, D.; Lu, G. *Adv. Mater.* **2014**, *26*, 3741.

(10) Guan, B. Y.; Yu, L.; Lou, X. W. *J. Am. Chem. Soc.* **2016**, *138*, 11306.

(11) Wang, Z.; Lou, X. W. *Adv. Mater.* **2012**, *24*, 4124.

(12) Liu, D.; Peng, X.; Wu, B.; Zheng, X.; Chuong, T. T.; Li, J.; Sun, S.; Stucky, G. D. *J. Am. Chem. Soc.* **2015**, *137*, 9772.

(13) Zoldesi, C. I.; Imhof, A. *Adv. Mater.* **2005**, *17*, 924.

(14) van Blaaderen, A. *Nature* **2006**, *439*, 545.

(15) Li, X.; Zhou, L.; Wei, Y.; El-Toni, A. M.; Zhang, F.; Zhao, D. *J. Am. Chem. Soc.* **2015**, *137*, 5903.

(16) Pei, F.; An, T.; Zang, J.; Zhao, X.; Fang, X.; Zheng, M.; Dong, Q.; Zheng, N. *Adv. Energy Mater.* **2016**, *6*, 1502539.

(17) Hyun, D. C.; Lu, P.; Choi, S.-I.; Jeong, U.; Xia, Y. *Angew. Chem., Int. Ed.* **2013**, *52*, 10468.

(18) Wang, Z.; Luan, D.; Li, C. M.; Su, F.; Madhavi, S.; Boey, F. Y. C.; Lou, X. W. *J. Am. Chem. Soc.* **2010**, *132*, 16271.

(19) Liu, J.; Wickramaratne, N. P.; Qiao, S. Z.; Jaroniec, M. *Nat. Mater.* **2015**, *14*, 763.

(20) Titirici, M.-M.; White, R. J.; Brun, N.; Budarin, V. L.; Su, D. S.; del Monte, F.; Clark, J. H.; MacLachlan, M. J. *Chem. Soc. Rev.* **2015**, *44*, 250.

(21) Roberts, A. D.; Li, X.; Zhang, H. *Chem. Soc. Rev.* **2014**, *43*, 4341.

(22) Lu, A.-H.; Hao, G.-P.; Sun, Q.; Zhang, X.-Q.; Li, W.-C. *Macromol. Chem. Phys.* **2012**, *213*, 1107.

(23) Schneider, G.; Decher, G. *Nano Lett.* **2004**, *4*, 1833.

(24) Lou, X. W.; Deng, D.; Lee, J. Y.; Archer, L. A. *Chem. Mater.* **2008**, *20*, 6562.

(25) Yoon, S. B.; Sohn, K.; Kim, J. Y.; Shin, C. H.; Yu, J. S.; Hyeon, T. *Adv. Mater.* **2002**, *14*, 19.

(26) Zhou, G. M.; Zhao, Y. B.; Manthiram, A. *Adv. Energy Mater.* **2015**, *5*, 1402263.

(27) Han, J.; Song, G.; Guo, R. *Adv. Mater.* **2006**, *18*, 3140.

(28) Xu, F.; Tang, Z.; Huang, S.; Chen, L.; Liang, Y.; Mai, W.; Zhong, H.; Fu, R.; Wu, D. *Nat. Commun.* **2015**, *6*, 7221.

(29) Wang, G.-H.; Sun, Q.; Zhang, R.; Li, W.-C.; Zhang, X.-Q.; Lu, A.-H. *Chem. Mater.* **2011**, *23*, 4537.

(30) Fan, J.; De bruyn, M.; Budarin, V. L.; Gronnow, M. J.; Shuttleworth, P. S.; Breeden, S.; Macquarrie, D. J.; Clark, J. H. *J. Am. Chem. Soc.* **2013**, *135*, 11728.

(31) Sun, X.; Li, Y. *J. Colloid Interface Sci.* **2005**, *291*, 7.

(32) Wen, Z.; Wang, Q.; Zhang, Q.; Li, J. *Electrochem. Commun.* **2007**, *9*, 1867.

(33) Titirici, M.-M.; Antonietti, M. *Chem. Soc. Rev.* **2010**, *39*, 103.

(34) Tang, M.; Deng, J.; Li, M.; Li, X.; Li, H.; Chen, Z.; Wang, Y. *Green Chem.* **2016**, *18*, 6082.

(35) Deng, J.; Xiong, T.; Xu, F.; Li, M.; Han, C.; Gong, Y.; Wang, H.; Wang, Y. *Green Chem.* **2015**, *17*, 4053.

(36) Ganguly, R.; Aswal, V. K.; Hassan, P. A.; Gopalakrishnan, I. K.; Kulshreshtha, S. K. *J. Phys. Chem. B* **2006**, *110*, 9843.

(37) Xin, X.; Xu, G.; Wang, Y.; Mao, H.; Zhang, Z. *Eur. Polym. J.* **2008**, *44*, 3246.

(38) Mai, Y.; Eisenberg, A. *Chem. Soc. Rev.* **2012**, *41*, 5969.

(39) Titirici, M.-M.; Antonietti, M.; Baccile, N. *Green Chem.* **2008**, *10*, 1204.

(40) Sevilla, M.; Fuertes, A. B. *Chem. - Eur. J.* **2009**, *15*, 4195.

(41) Shibata, J.; Fuerstenau, D. W. *Int. J. Miner. Process.* **2003**, *72*, 25.

(42) Mortensen, K.; Pedersen, J. S. *Macromolecules* **1993**, *26*, 805.

(43) Wanka, G.; Hoffmann, H.; Ulbricht, W. *Macromolecules* **1994**, *27*, 4145.

(44) Vliegenthart, G. A.; Gompper, G. *New J. Phys.* **2011**, *13*, 045020.